Accurate Born–Oppenheimer Calculations of the Low-Lying $c^3\Sigma_g^+$ and $a^3\Sigma_u^+$ Excited States of Helium Dimer

MICHELE PAVANELLO,[1] MAURICIO CAFIERO,[2] SERGIY BUBIN,[1] LUDWIK ADAMOWICZ[1]

[1]*Department of Chemistry, University of Arizona, Tucson, AZ 85721*

[2]*Department of Chemistry, Rhodes College, Memphis, TN 38112*

Received 24 March 2008; accepted 25 March 2008
Published online 27 May 2008 in Wiley InterScience (www.interscience.wiley.com).
DOI 10.1002/qua.21757

ABSTRACT: Accurate variational Born–Oppenheimer calculations of the two lowest excited Σ triplet states of the helium dimer at their respective equilibrium geometries are reported. The wave functions of the states are expanded in terms of explicitly correlated Gaussian functions with shifted centers. The obtained energies are the best variational estimates ever calculated for these states. One-electron densities are also presented and discussed. The results are compared with the experimental values and previous calculations. © 2008 Wiley Periodicals, Inc. Int J Quantum Chem 108: 2291–2298, 2008

Key words: helium dimmer; Born–Oppenheimer; nonrelativistic; excited states; correlated Gaussians

1. Introduction

Since 1929, with the early work of Hylleraas [1] on the helium atom, the approach to calculating the bound states of atomic and molecular systems based on directly including the dependency on the interelectronic distances in the wave function has led to important benchmark results. One of the most popular types of basis functions in such calculations in the past 20 years have been the so-called explicitly correlated Gaussian functions (ECGs). ECGs have been employed in various types of studies ranging from very accurate calculations of atomic energy levels to calculations of potential energy surfaces of small diatomic and triatomic molecules and clusters. For the original works concerning ECGs we refer the reader to the papers by Boys [2] and Singer [3], while the most recent works describing very accurate Born–Oppenheimer molecular calculations with ECGs can be found in [4–7] and references therein. There have been also some high-accuracy molecular calculations with

Correspondence to: M. Pavanello; e-mail: pavanell@email.arizona.edu

Contract grant sponsors: Merck Research Laboratories, National Science Foundation, High Performance Computing Center at the University of Arizona.

© 2008 Wiley Periodicals, Inc.

ECGs where the BO approximation was not assumed [8–10]. In general, the convergence of calculations carried out using ECGs is reasonably fast for the total energy, but somewhat slower for other properties [11]. This particularly applies to properties whose operators are sensitive to how well the cusp conditions are represented in the wave function. These conditions are usually more difficult to describe using the Gaussian-type functions than the Slater-type functions. However, it is not yet possible to employ the Slater functions to perform high-accuracy molecular calculations due to the complexity of the Hamiltonian matrix elements with those functions, which have not yet been derived for the general case [12]. The use of the correlated Gaussians on the other hand leads to much simpler expressions for the matrix elements even for functions where several electrons are explicitly correlated at the same time. The ability of the ECGs to describe the cusp conditions can be improved by the inclusion of pre-multipliers dependent upon the first power of the interparticle distances, but this complicates the algorithms for the multiple-electron matrix elements and their implementation [13, 14].

In this work we expand the electronic wave function in terms of ECGs with shifted centers to carry out single-point energy calculations of the two lowest Σ triplet states of the helium dimer. In the calculations the wave function is obtained variationally through the minimization of the energy with respect to the linear and nonlinear (the exponents and the shifts of the Gaussians) parameters. The wave function in our calculations has the following form:

$$\Psi = \sum_{k=1}^{M} c_k \phi_k, \tag{1}$$

where M is the size of the basis set, c_k are the linear coefficients, and the ϕ_k are ECGs:

$$\phi_k = \exp[-(\mathbf{r} - \mathbf{s}_k)'(\mathbf{A}_k \otimes \mathbf{I}_3)(\mathbf{r} - \mathbf{s}_k)]. \tag{2}$$

In (2), I_3 is the 3×3 identity matrix, 196 stands for the Cartesian Kroneker product operation, and $\mathbf{r}$ and $\mathbf{s}_k$ are $3N$ dimensional vectors, where N is the number of electrons. $\mathbf{r}$ is the vector of the Cartesian coordinates of the positions of the electrons, $\mathbf{s}_k$ is the vector of the shifts of the Gaussian centers, and $\mathbf{A}_k$ is a $N \times N$ symmetric matrix of the Gaussian exponents. The elements of the $\mathbf{A}_k$ matrix and the $\mathbf{s}_k$ vector are the nonlinear parameters that are variationally optimized in the calculation. The Hamiltonian matrix elements with functions (2), and their derivatives with respect to the nonlinear parameters, were derived in the previous work of our group [15]. We use them to determine the total energy and the energy gradient in the present calculations. The use of the analytical gradient in the variational energy minimization [16] is the main difference between the approach used in this work and the methods used by others [4]. There is also a difference in the way we handle the optimization of the elements of the $\mathbf{A}_k$ matrix. In our approach we use the following Cholesky factorization [17] of this matrix in terms of a lower triangular matrix $\mathbf{L}_k$: $\mathbf{A}_k = \mathbf{L}_k'\mathbf{L}$. With such a factorization and with the use of the elements of the L_k matrix as variational parameters, the optimization of the energy functional can be performed without any restrictions on the range of the variables. Such restrictions would need to be imposed, if the variational parameters were the elements of the $\mathbf{A}_k$ matrix, which needs to be positive definite in order for the Gaussian to be a square-integrable function. We note that the positively definite character of the $\mathbf{A}_k$ matrix does not preclude some of its elements from being negative.

In this work we have developed a new computational code for molecular calculations with ECGs. We first tested the new code by performing calculations on the ground state ($^1S_0$) and the first excited state ($^3S_1$) of the helium atom. Next we performed calculations on the $c^3\Sigma_g^+$ and $a^3\Sigma_u^+$ states of the helium dimer at their respective equilibrium distances. The test atomic calculations were done to compare our results with the existing high-accuracy calculations. The calculations on the triplet states of the helium dimer were performed because of their relevance to properties of liquid helium [18], and these states have not been described before with the accuracy achieved in this work.

2. Method Used in the Calculations

In the calculations we used the variational method to determine the energies and the wave functions of the studied systems. The minimization of the Rayleigh quotient:

$$E = \frac{\langle \Psi | H | \Psi \rangle}{\langle \Psi | \Psi \rangle} \tag{3}$$

was employed and both linear and nonlinear parameters of the wave function were optimized. The linear parameters were determined by solving the secular equation: $(\mathbf{H} - \epsilon\mathbf{S})\mathbf{c} = \mathbf{0}$ and the nonlinear parameters were optimized using the optimization routine TN [19] developed by Nash. This routine was specifically developed to perform an unconstrained minimization of a multivariable function. The routine uses the analytical gradient of the minimized function calculated with respect to the nonlinear parameters. In the present calculations, the analytical gradient of the Rayleigh ratio was determined using the procedures developed previously by our group [16]. Although, in principle, the use of the TN routine seems straightforward, in practice it becomes less effective when the ECG basis size becomes larger than ≈300 functions. When using over 300 functions, the number of nonlinear parameters approaches 7,000, and because of the coupling between the basis functions and the high degree of the nonlinearity of the problem, it becomes difficult to further lower the energy in the minimization process. Furthermore, when the number of basis functions becomes large, linear dependencies between the basis functions arise more frequently often leading to an increase of the numerical inaccuracy. To overcome these problems we have modified the optimization approach by (a) implementing a routine to partition the basis into smaller subsets of functions and to optimize only a single subset at a time; (b) implementing a routine for incremental enlarging of the basis set by a small number of functions and for optimizing the whole set each time a new subset of functions is added to the basis set; (c) implementing a routine to check linear dependencies in the basis set and to remove them either by eliminating the functions that cause them or by shifting their nonlinear parameters to move the functions apart. The approach was tested in the calculations for the ground $^1S_0$ and the first excited $^3S_1$ state of the helium atom, and after some tuning, the procedure was coded for the general use. The helium calculations were also needed to evaluate the dissociation limits of the helium dimer.

Another important development in this work has been the implementation of the spatial and permutational symmetry in the calculation. This was done by using projectors onto the chosen irreducible representation of the group $S_N \otimes P$, where here $\otimes$ is the tensor product, S_N is the finite permutational symmetry group of N elements, and P is the point symmetry group of the molecular system under consideration. The symmetry procedure implemented in our program requires a Young frame [20, 21] as the input, and as the output it gives the elements of the Young projector $\hat{Y}$ to be applied to the $\mathbf{A}_k$ matrices of the basis functions.

The implementation of the point group symmetry required the use of the projector $\hat{P}$ defined as follows. We first define the projectors $\hat{Y} = 1/N! \sum_{i=1}^{N!} \chi_i^Y \hat{O}_i$ and $\hat{P} = 1/g \sum_{j=1}^{g} \chi_j^P \hat{O}'_j$, where N is the number of electrons and g is the order (the number of elements) of the point group, χ_i^Y and χ_j^P are the elements of the matrices of the irreducible representation necessary to build the projectors, and $\hat{O}_i$ and $\hat{O}'_j$ are the elements of the permutational and point group symmetries, respectively. With that we can write the general form of the projector $\hat{Y}\hat{P}$ as

$$\hat{Y}\hat{P} = \frac{1}{N!g} \sum_{i=1}^{N!} \sum_{j=1}^{g} \chi_i^Y \chi_j^P (\hat{O}_i \cdot \hat{O}'_j). \qquad (4)$$

For homonuclear diatomic molecules, the symmetry point group ($D_{\infty h}$) is not finite. In this case it was necessary to restrict the shifts $\mathbf{s}_k$ in the Gaussians to lie on the line that interconnects the nuclei and then to apply the projector corresponding to the C_i point group, which is $\hat{P}_{\pm} = 1/2\,(\hat{E} \pm \hat{I})$, where $\hat{E}$ is the identity operation and $\hat{I}$ is the inversion. The projector $\hat{P}_+$ is used to generate *gerade* wave functions, while $\hat{P}_-$ is used to generate *ungerade* wave functions.

3. Results and Discussion

As mentioned, the calculations of the helium dimer have been performed for the $c^3\Sigma_g^+$ and $a^3\Sigma_u^+$ excited states of this system at their respective equilibrium internuclear distances of $R_e = 2.080$ and 1.976 a.u. The total nonrelativistic energy has been computed for several basis sets of different lengths, M, ranging from $M = 35$ to 400. In the test calculations for the helium atom, the basis set size ranged from $M = 30$ to 200. These numbers correspond to the basis-set sizes before the symmetry projections are applied. The inclusion of the projectors of the point group symmetry and the permutational symmetry, to each basis function, effectively increases the basis set size for the helium atom from 200 to 400, and for the helium dimer from 400 to 19,200. Generally, the implementation of the punctual symmetry group in the calculation results in an increase

TABLE I

Total energies of the helium atom and the helium dimer.

	This work	Best in the literature
He $^1S_0$	−2.90372437	−2.90372438 [23]
He $^3S_1$	−2.17522937	−2.17522938 [23]
He_2 $a^3\Sigma_u^+$	−5.15043942	−5.142 [26]
He_2 $c^3\Sigma_g^+$	−5.09943867	−5.088 [26]

Energy values are in a.u.

in the number of basis functions by a factor that is equal to the group order [22].

In Table I we show the total energies obtained in the calculations and we compare them with the best nonrelativistic energies available in the literature. For the test helium calculations the energies are reproduced up to the seventh decimal digit with respect to the nonrelativistic limit [23]. This is an indication that our approach works well for a two-electron system, giving reason to expect that it will also work well for a system with four electrons. In the table, we also show the results for the helium dimer. In this case the only literature results that we have been able to find were obtained using the orbital approximation and standard post-Hartree–Fock methods (such as the coupled-cluster method). These methods are not variational and the comparison with our variational results is not fully meaningful. Nevertheless, the difference of about 10^{-2} Hartree between our results and the best available calculations for the helium dimer (our results being lower) clearly indicates the use of ECGs in our approach leads to much better results. This is consistent with previous assessments about the relatively low accuracy level of the one-electron (orbital) approximation (see, for example, [5]).

In Tables II and III we show how the total energies converge with the basis set size. Generally, the convergence is fast for all the states considered. It is important to mention, however, that starting from $M = 200$ functions the full optimization of the dimer wave function with respect to all nonlinear parameters was replaced with a "fragmented" optimization approach. In this approach the basis set was divided in groups of 50 functions and each group was optimized separately from the other groups.

In the atomic helium calculations, the singlet converged somewhat faster than the triplet. This can be attributed to the difference in the electron correlation effects for these two states, hence affecting the ability of the ECGs to describe them. In Figure 1(a), we show a plot of the one-electron densities for the two states determined using the ECG wave functions calculated in this work. The singlet shows a higher density around the nucleus while the density for the triplet states is more spread out, as can be seen in Figure 1(b). These peculiarities of the density are the result of the existence of a Fermi hole between two electrons with the same spin (the triplet state) and lack of a Fermi hole for two electrons with the same spin (the singlet state), which makes the electrons in the latter case approach each other, on average, closer than in the former case.

In Figure 2, we show plots of one-electron densities for the $c^3\Sigma_g^+$ and $a^3\Sigma_u^+$ states of He_2. The plots correspond to the densities calculated along the internuclear axis. As expected, the density for the higher energy $c^3\Sigma_g^+$ state is more spread out than for the lower-energy $a^3\Sigma_u^+$ state. In addition, the *ungerade* state has a substantial density in the mid-

TABLE II

Convergence of the total energy of the $^1S_0$ and $^3S_1$ states of atomic Helium with respect to the basis size.

M	$E_{^1S_0}$	$E_{^3S_1}$
30	−2.9037038	−2.1752228
50	−2.9037220	−2.1752288
60	−2.9037238	−2.1752292
80	−2.9037242	−2.1752293
200	−2.9037244	−2.1752294

Energy values are in a.u.

TABLE III

Covergence of the total energy of the $c^3\Sigma_g^+$ and $a^3\Sigma_u^+$ states of Helium dimer with respect to the basis size.

M	$E_{c^3\Sigma_g^+}$	$E_{a^3\Sigma_u^+}$
35	−5.0791717	−5.1406466
65	−5.0893536	−5.1466806
95	−5.0951381	−5.1486696
150	−5.0978387	−5.1501089
200	−5.0992452	−5.1504074
400	−5.0994387	−5.1504394

Energy values are in a.u.

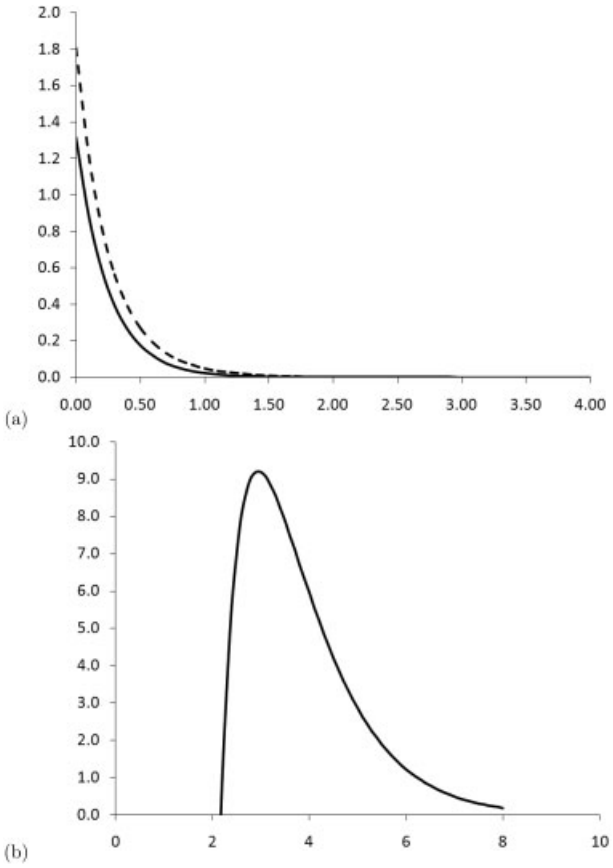

FIGURE 1. (a) Radial one-electron densities of the $^1S_0$, dashed line, and the $^3S_1$ states of atomic Helium calculated with the 200-term ECG wave function. (b) Difference between the one-electron densities of the $^3S_1$ and $^1S_0$ states of atomic Helium calculated with the 200-term ECG wave function, zoom between $r = 2$ and 8 au. The density (y-axis) and the position (x-axis) are in atomic units.

point between the atoms, which is larger than the midpoint density of the *gerade* state. This follows the common idea of a chemical bond: the higher the density in between the atoms, the stronger the bond. This simple reasoning accounts for the higher stability of the *ungerade* state. A derivation of the one-electron density matrix elements with ECGs, which has never been presented before, is shown in the Appendix.

Experiments on the lowest triplet states of the helium dimer have been carried out by Focsa et al. [24]. They identified and measured many spectral lines corresponding to several states of this system. They determined that v_e of the $c^3\Sigma_g^+ - a^3\Sigma_u^+$ transition (that would be the energy separation between the bottom of the potential energy surfaces of the $c^3\Sigma_g^+$ and the $a^3\Sigma_u^+$ states as defined on page 151 of Ref. [25]) to be 1.364278(9) eV. The coupled-cluster calculations [26] predicted $\nu_e(c^3\Sigma_g^+ - a^3\Sigma_u^+) = 1.47$ eV, which is about 8% higher than the experimental value.

The energy results obtained in the present calculations are plotted in Figure 3. In Figure 3(a), we show how $\nu_e(c^3\Sigma_g^+ - a^3\Sigma_u^+)$ converges with respect to the number of basis functions. The plot (a) also shows that $\nu_e(c^3\Sigma_g^+ - a^3\Sigma_u^+)$ converges from the above toward the experimental value. This indicates that for equal basis set sizes, the *ungerade* state (lower in energy) has energy closer to its exact value than the *gerade* state. As mentioned earlier, this is due to the fact that different numbers of functions may be needed for different states to achieve an equivalent convergence level for the total energy. In addition, Figure 3(a) features a trend line which has been generated via a least-squares fitting using the exponential function: $f(M) = a + be^{-cM}$, where the parameter a corresponds to the asymptotic limit of $\nu_e(c^3\Sigma_g^+ - a^3\Sigma_u^+)$. The fitted parameters were determined to be $a = 1.386 \pm 0.011$ eV, $b = 0.581 \pm 0.065$ eV, and $c = -0.020 \pm 0.003$, where the error bars are one standard deviation (σ). The experimental value falls within two standard deviations of the asymptotic limit that we obtained. According to Ref. 25 (pages 99 and 100), the binding energies, D_e, of the two states of He_2 dimer considered here are defined as

$$D_e\left(a^3\Sigma_u^+\right) = E_{a^3\Sigma_u^+} - [E_{1S_0} + E_{3S_1}].$$

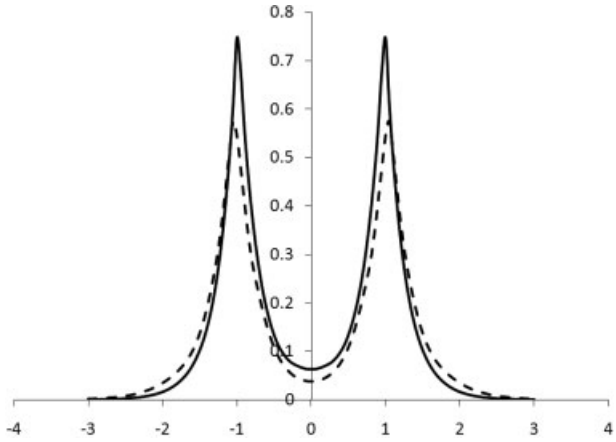

FIGURE 2. One-electron densities, along the internuclear axis, of the $c^3\Sigma_g^+$, dashed line, and $a^3\Sigma_u^+$ excited states of Helium dimer calculated with the 400-term ECG wave function. The density (y-axis) and the position (x-axis) are in atomic units.

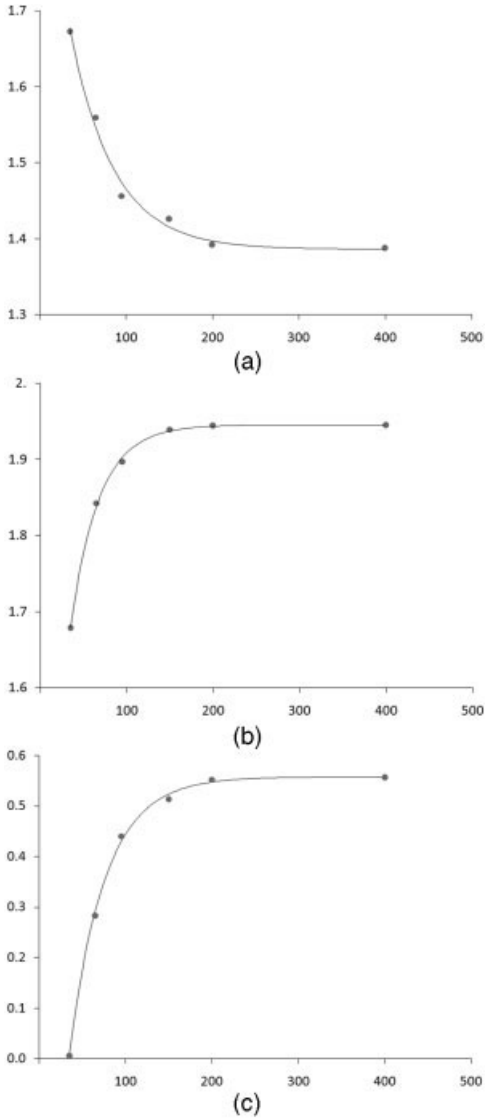

FIGURE 3. Convergence of the difference of the total energies (v_e) of the $c^3\Sigma_g^+$ and $a^3\Sigma_u^+$ states of Helium dimer (a); binding energies (D_e) of the *gerade* state (b), and *ungerade* state (c), with respect to the basis-set size (M). Energy values are in eV. The superimposed trend line has been generated by a least square fitting using the function $f(M) = a + be^{-cM}$.

$$D_e\left(c^3\sum_g^+\right) = E_{c^3\Sigma_g^+} - [E_{1_{S_0}} + E_{3_{S_1}}].$$

In Figures 3(b) and (c), we included plots showing how the binding energy for each state converges with the increasing size of the basis set. These plots also feature the corresponding trend lines generated using the $f(M)$ exponential function. $D_e(c^3\Sigma_g^+) = 0.558 \pm 0.007$ eV and $D_e(a^3\Sigma_u^+) = 1.946 \pm 0.003$ eV are the extrapolated binding energies. The reported uncertainties are equal to the corresponding σ values. The previous calculations [26] estimated the two binding energies to be $D_e(c^3\Sigma_g^+) = 0.40$ eV, and $D_e(a^3\Sigma_u^+) = 1.88$ eV. Earlier variational calculations by Poshusta [27] and Beck [28] on the $a^3\Sigma_u^+$ state yielded the binding energy of about 0.9 eV. Because in this work we exploit the variational theorem, our binding energies are lower bounds of the true values. The fact that our binding energies are noticeably lower than the values found in the literature shows that this work is significantly more accurate than the previous calculations.

4. Conclusions and Future Directions

In this work we report first the high-accuracy calculations of the helium dimer in the two lowest Σ triplet states. The calculated variational energies are the best results ever obtained for these states. The calculations have been performed with our new computer code where the explicit treatment of the molecular symmetry was implemented. The code was first tested in benchmark calculations for the helium atom. The work also includes a derivation of the matrix elements for calculating one-electron densities with the ECG functions. The algorithm was applied to describe the difference between the electron distribution in the two triplet states of the helium dimer. The one-electron density matrix elements constitute the starting point for the evaluation of other one-electron molecular properties. These include the electric field, the electric field gradient, and the electron spin density. Our future work will involve the calculation of these properties with our computer code.

The result obtained for the energy separation between the $c^3\Sigma_g^+$ and $a^3\Sigma_u^+$ states is about 1.5% off the experiment. This indicates that more work needs to be done in order to improve the approach used for the variational optimization of the wave function and for calculating the energy. The results show that a larger number of basis functions ($M >$ 400) is need to achieve spectroscopic accuracy.

Appendix: One-Electron Density

INITIAL DEFINITIONS

The total wave function is defined in terms of ECGs,

$$\Psi = \sum_{k=1}^{M} c_k g_k, \tag{A1}$$

where M is the size of the basis set. Each ECG g_k (or g_t) can be written as follows:

$$g_k = \exp[-(r - s_k)'\bar{A}_k(r - s_k)]. \tag{A2}$$

where, if n_e is the number of electrons, r, s_k, and s_l are $3n_e$-dimensional vectors; here any overlined matrix, for instance $\bar{A}_k$, is a $3n_e \times 3n_e$ matrix that would be the Kroneker product $A_k \otimes I_3$ [6], where A_k is a $n_e \times n_e$ matrix and I_3 is the identity in the three-dimensional space. The multiplication of g_k and g_l leads to

$$g_k \cdot g_l = \lambda_{kl} \exp[-r'\bar{A}_{kl}r + 2b'_{kl}r], \tag{A3}$$

where $\lambda_{kl} = \exp[-s'_k\bar{A}_k s_k - s'_l\bar{A}_l s_l]$, $\bar{A}_{kl} = \bar{A}_k + \bar{A}_l$, and $b'_{kl} = s'_k\bar{A}_k + s'_l\bar{A}_l$.

RULE FOR INTEGRATION

Given two vectors x and z of dimension n, and a square matrix $n \times n$ M, we can solve the following integral:

$$\int_{-\infty}^{+\infty} \exp[-x'Mx + z'x]dx_1dx_2\ldots dx_n = \left(\frac{\pi^n}{|M|}\right)^{1/2} \exp\left[\frac{z'M^{-1}z}{4}\right]. \tag{A4}$$

ONE-ELECTRON DENSITY INTEGRAL

The one-electron density at the point in space ξ is the expectation value of the one-electron operator $\delta(r_i - \xi)$. Namely,

$$\langle\delta(r_i - \xi)\rangle = \frac{\langle\Psi|\delta(r_i - \xi)|\Psi\rangle}{\langle\Psi|\Psi\rangle}, \tag{A5}$$

and applying Eq. (A1), we get

$$\langle\delta(r_i - \xi)\rangle = \frac{\sum_{k,l} c_k c_l \langle g_k|\delta(r_i - \xi)|g_l\rangle}{\sum_{k,l} c_k c_l \langle g_k|g_l\rangle}. \tag{A6}$$

The matrix elements of the delta function are

$$\langle g_k|\delta(r_i - \xi)|g_l\rangle = \lambda_{kl} \exp[-a_{kl}\xi^2 + 2u'\xi] \times \int_{-\infty}^{+\infty} \exp[-r'^{(i)}\bar{D}_{kl}r^{(i)} + 2(b_{kl}^{(i)} - \xi q_k)'r^{(i)}]\, dr_1\ldots dr_{i-1}\, dr_{i+1}\ldots dr_{n_e}, \tag{A7}$$

where δ is the Dirac delta; r_i is a 3-dimentional vector, the position of the ith electron; $r^{(i)}$ is a $(3n_e - 3)$-dimensional vector, the $\mathbf{r}$ vector without the ith dimension; ξ is a three-dimensional vector, the point in space where the density is evaluated; a_{kl} is the ith diagonal element of A_{kl}; u is a three-dimensional vector composed by the $(3i + 1)$, $(3i + 2)$, and $(3i + 3)$-rd element of the b_{kl} vector; D_{kl} is a $(n_e - 1) \times (n_e - 1)$ matrix, the A_{kl} matrix without the ith dimension; q_{kl} is a $(n_e - 1)$-dimensional vector composed by the ith column of A_{kl} without the ith element; $b_{kl}^{(i)}$ is a $(3n_e - 3)$-dimensional vector composed by b_{kl} without the $(3i + 1)$, $(3i + 2)$, and $(3i + 3)$ elements.

Applying Eq. (A4), we finally get

$$\langle g_k|\delta(r_i - \xi)|g_l\rangle = \lambda_{kl}\left(\frac{\pi^{n_e-1}}{|D_{kl}|}\right)^{3/2} \exp[\gamma'\bar{D}_{kl}^{-1}\gamma] \exp[-a_{kl}\xi^2 + 2u'\xi], \tag{A8}$$

where $\gamma = b_{kl}^{(i)} - \xi q_{kl}$, where the product ξq_{kl} is a $3 \times (n_e - 1)$-dimensional vector defined as $(\xi q_{kl})_{[(l-1)+k]} = \xi_k(_{kl})_l$.

Because we assume g_k and g_l to be normalized, we need to modify Eq. (A8) accordingly:

$$\frac{\langle g_k|\delta(r_i - \xi)|g_l\rangle}{\sqrt{\langle g_k|g_k\rangle\langle g_l|g_l\rangle}} = \lambda_{kl}\left(2^{n_e}\frac{|A_k|^{1/2}|A_l|^{1/2}}{\pi|D_{kl}|}\right)^{3/2} \exp[\gamma'\bar{D}_{kl}^{-1}\gamma] \exp[-a_{kl}\xi^2 + 2u'\xi]. \tag{A9}$$

Now we can plug the matrix element just found into Eq. (A6) and obtain the one-electron density in the point ξ.

ACKNOWLEDGMENT

The authors thank Emily Tenenbaum for editing this manuscript.

References

1. Hylleraas, E. A. Z Phys 1929, 54, 347.
2. Boys, S. F. Proc R Soc Lond Ser A 1960, 258, 402.
3. Singer, K. Proc R Soc London Ser A 1960, 258, 412.
4. Cencek, W. J Chem Phys 1993, 98, 1252.
5. Komasa, J.; Rychlewski, J. Chem Phys Lett 1996, 249, 253.
6. Cafiero, M.; Adamowicz, L. Chem Phys Lett 2001, 335, 404.
7. Komasa, J. Mol Phys 2006, 104, 2193.
8. Kinghorn, D. B.; Adamowicz, L. J Chem Phys 1999, 110, 7166.
9. Kinghorn, D. B.; Adamowicz, L. Phys Rev Lett 1999, 83, 2541.
10. Cafiero, M.; Adamowicz, L. Phys Rev Lett 2002, 88, 033002.
11. Stanke, M.; Kedziera, D.; Molski, M.; Bubin, S.; Barysz, M.; Adamowicz, L. Phys Rev Lett 2006, 96, 233002.
12. Safouhi, H.; Bouferguene, A. Theor Chem Acc 2007, 117, 213.
13. Pachucki, K.; Komasa, J. Chem Phys Lett 2004, 389, 209.
14. Klopper, W.; Kutzelnigg, W, W. J Chem Phys 1991, 94, 2020.
15. Bubin, S.; Cafiero, M.; Adamowicz, L. In Advances in Chemical Physics, Vol. 131; Wiley: New Jersey, 2005; p 377.
16. Cafiero, M.; Adamowicz, L. Int J Quantum Chem 2001, 82, 151.
17. Kinghorn, D. B. Int J Quantum Chem 1996, 57, 141.
18. Jordan, R. M.; Siddiqui, H. R.; Siska, P. E. J Chem Phys 1986, 84, 6719.
19. Nash, S. G. SIAM J Numer Anal 1984, 21, 770.
20. Pauncz, R. Spin Eigenfunctions; Springer-Verlag: Berlin, 1979.
21. Hamermesh, M. Group Theory and Its Application to Physical Problems; Dover: New York, 1962.
22. Wigner, E. P. Group Theory and its Application to the Quantum Mechanics of Atomic Spectra; Academic Press: New York, 1971.
23. Drake, G. W. F.; Yan, Z. Chem Phys Lett 1994, 229, 486.
24. Focsa, C.; Bernath, P. F.; Colin, R. J Mol Spect 1998, 191, 209.
25. Herzberg, G. Molecular Spectra and Molecular Structure. I. Spectra of Diatomic Molecules, 2nd ed.; Van Nostrand Reinhold: New York, 1950.
26. Minaev, B. Phys Chem Chem Phys 2003, 5, 2314.
27. Poshusta, R. D.; Matsen, F. A. Phys Rev, 1969, 132, 307.
28. Beck, D. B.; Nicolaides, C. A.; Musher, J. I. Phys Rev A 1974, 10, 1522.